A Model for Ion Transport across Membranes: Solution Structure of the Ionophore Metal Complex Salinomycin–Na Determined by NMR and Molecular Dynamics Calculations

Siggi Mronga,*,†,‡ Gerhard Müller,†,⊥ Jacob Fischer,† and Frank Riddell§

Contribution from the Organisch-Chemisches Institut, Technische Universität München, Lichtenbergstrasse 4, D-8046 Garching, Germany, and Deparment of Chemistry, The University of St. Andrews, St. Andrews KY16 9ST, Scotland

Received February 23, 1993

Abstract: The conformational analysis of the ionophore metal complex salinomycin–Na by NMR spectroscopy and molecular dynamics (MD) calculation was carried out in solution to study a model for ion transport across biological membranes. The first NMR solution structure of an ionophore metal complex using NOE-derived distances is reported. The 51 distance constaints derived from a 600-MHz NOESY spectrum of this molecule in the extreme narrowing limit were in agreement with an overall macrocyclic solution structure. The back-calculation of the NOESY spectrum confirmed the reliability of the NOE data. The structure was first refined by MD simulation *in vacuo* without a sodium ion present and subsequently in solution in the presence of a sodium ion. The complex shows a hydrophobic surface and a hydrophilic core, with the ion coordinated by a distorted pentagonal pyramid of oxygen atoms. Additional free MD simulations with and without the ion provide further information about the exact hinge regions and a possible mechanism of ionophoric action.

Introduction

Ionophores are of great importance for the mediation of ion transport through biological membranes,[1] and interest in the conformation of ionophores has considerably increased.[2-9] Many ionophores are in current use, particularly as veterinary pharmaceuticals such as the following very effective anticoccidials and antibiotics: lasalocid (Avatec), monensin (Elancuban, Rumensin), narasin (Monteban), and salinomycin (Sarox, Biocox, Coxistac, Salocin).[10,11]

Presently very little is known about the biologically active conformations of ionophores. It is clear, however, that the conformational analysis of ionophore metal complexes is an indispensible tool for understanding the mechanism of the transport.

X-ray structures exist for almost all types of ionophores.[1] For several ionophores such as valinomycin,[12,13] enniatin,[14] and monensin,[2,15] the conformations in the solid state of uncomplexed and alkali metal-complexed ionophores are known.[1] For valinomycin the X-ray structure and the conformational analysis in solution of the K^+ complex led to similar results,[16-19] which showed the K^+ ion to be coordinated by six carbonyl oxygens.

NMR spectroscopy is one of the most effective methods for investigating the conformation and dynamics of biomolecules.[20-30] However, no solution structure of any alkali metal ionophore complex has been obtained using NMR-derived distances[30] for structure calculation. This paper demonstrates how the combined use of current 2D NMR techniques and molecular dynamics (MD) calculations *in vacuo* and in solution delivers a detailed insight into the solution-state structure of the carboxylic ionophore metal complex salinomycin–Na. Salinomycin[31] (Figure 1) was chosen because it is known to form a macrocyclic structure by head-to-tail hydrogen bonding, as is typical for carboxylate ionophores.[33-36] A crystal structure exists only for a salinomycin derivative,[37] which is unable to form a macrocycle due to its derivatization. The ion complex should represent an excellent

† Technische Universität München.
‡ Present address: Institut für Molekularbiologie und Biophysik, Eidgenössische Technische Hochschule, 8093 Zürich, Switzerland.
§ The University of St. Andrews.
⊥ Present address: Glaxo S.p.A., Research Centre Medicinal Chemistry, I-37100 Verona, Italy.

(1) Dobler, M. *Ionophores and Their Structures*; John Wiley & Sons, Inc.: New York, 1981.
(2) Lutz, W. K.; Winkler, F. K.; Dunitz, J. D. *Helv. Chim. Acta* **1971**, *54*, 1103–1108.
(3) Braunias, W. W. *World's Poult. Sci. J.* **1985**, *41*, 198–209.
(4) Riddell, F. G.; Tompsett, S. T. *Biochem. Biophys. Acta* **1990**, *1024*, 193–197.
(5) Anteunis, M. J. O.; Rodios, N. A. *Bull. Soc. Chim. Belg.* **1981**, *90*, 715–735.
(6) Riddell, F. G.; Tompsett, S. T. *Tetrahedron* **1991**, *47*, 10109–10118.
(7) Anteunis, M. J. O.; Rodios, N. A. *Bull. Soc. Chim. Belg.* **1981**, *90*, 449–480.
(8) Ovchinnikov, Y. A.; Ivanov, V. T.; Shkrob, A. M. *Membrane Active Complexones*; Elsevier Scientific Publishing Company: Amsterdam, 1974.
(9) Anteunis, M. J. O.; Seto, H.; Otake, N. *Polyether Antibiotics*; Westley, J. W., Ed.; Marcel Dekker, Inc.: New York, 1982.
(10) Harms, R. H.; Ruiz, W.; Buresh, R. E. *Poult. Sci.* **1989**,*68*, 86–88.
(11) Volz, S. D.; Lee, B. L.; Nowakowsky, L. H.; Conder, G. A. *Vet. Parasitol.* **1988**, *28*, 1–9.
(12) Duax, W. L.; Hauptmann, H.; Weeks, C. M.; Norton, D. A. *Science* **1972**, *176*, 911–914.
(13) Pinkerton, M.; Steinrauf, L. K.; Dawkins, P. *Biochim. Biophys. Res. Commun.* **1969**, *35*, 512–518.
(14) Ivanov, V. T.; Evstranov, A. V.; Sumskaya, L. V.; Melnik, E. I.; Chumburidze, T. S.; Portnova, S. L.; Balashova, T. A.; Ovchiinnikov, Yu. A. *FEBS Lett.* **1973**, *36*, 65–71.
(15) Pinkerton, M.; Steinrauf, L. K. *J. Mol. Biol.* **1970**, *49*, 533–546.
(16) Ivanov, V. T.; Laine, I. A.; Abdulaev, N. D.; Senyavina, L. B.; Popovi, E. M.; Ovchinnikov, Yu. A.; Shemyakin, M. M. *Biochem. Biophys. Res. Commun.* **1969**, *34*, 803–811.
(17) Onishi, M.; Urry. D. W. *Science* **1970**, *168*, 1091–1092.
(18) Patel, D. J.; Tonelli, A. E. *Biochemistry* **1973**, *12*, 486–496.
(19) Patel, D. J. *Biochemistry* **1973**, *12*, 496–501.
(20) Wüthrich, K. *NMR of Proteins and Nucleic Acids*; Wiley: New York 1986.
(21) Ernst, R. R.; Bodenhausen, G.; Wokaun, A. *Principles of Nuclear Magnetic Resonance in One and Two Dimensions*; Clarendon: Oxford, 1987.
(22) Kessler, H.; Gerke, M.; Griesinger, C. *Angew. Chem., Int. Ed. Engl.* **1988**, *27*, 490–536.
(23) Wagner, G. *Prog. Nucl. Magn. Reson. Spectrosc.* **1990**, *22*, 101–139.
(24) Patel, D. J.; Shapiro, L.; Hare, D. *Q. Rev. Biophys. Chem.* **1987**, *16*, 423–454.
(25) Clore, G. M.; Gronenborn, A. M. *Prog. Nucl. Magn. Reson. Spectrosc.* **1991**, *23*, 43–92.
(26) Wright, P. E. *TIBS* **1989**, *14*, 255–260.
(27) Bax, A. *Annu. Rev. Biochem.* **1989**, *58*, 223–256.
(28) Markley, J. L. *Methods Enzymol.* **1989**, 176, 12–64.
(29) Fesik, S. W.; Zuiderweg, E. R. *Q. Rev. Biophys.* **1990**, *23*, 97–131.
(30) Neuhaus, D.; Williamson, M. *The Nuclear Overhauser Effect*; VCH: New York, 1989.
(31) Kinashi, H.; Otake, N.; Yonehara, H. *Tetrahedron Lett.* **1973**, 4955–4958.
(32) Westley, J. W. *J. Antibiot.* **1976**, *29*, 584–586.
(33) Kinashi, H.; Otake, N.; Yonehara, H.; Satos, S.; Saito, Y. *Acta Crystallogr.* **1975**, *B31*, 2411–2415.

0002-7863/93/1515-8414$04.00/0

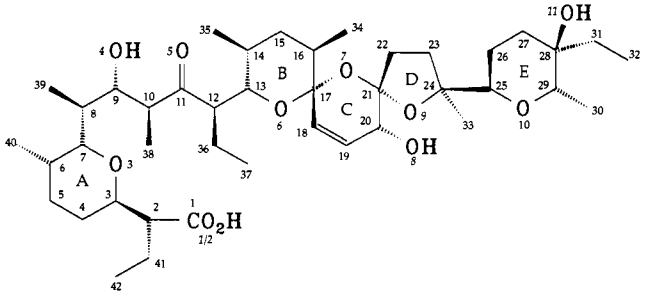

Figure 1. Constitution of salinomycin. The torsion notation is not in agreement with the Cahn–Ingold–Prelog sequence rules. The dihedrals along the longest carbon backbone skeleton, starting at C1 and ending at C30. These so called "master torsions" [32] are different from, e.g., the ring torsions, taking the higher preference of oxygen atoms into account when following the CIP rules. The master torsion definition is commonly used in most of the previously published works[5,6] concerning carboxylic ionophores as well as the numbering notation introduced by Westley.[32]

model substance to study the "captured metal" which is known to be transported in the inside of an "oildrop", with the hydrophobic outside of the salinomycin macrocycle representing this oildrop. Here, we report the structure determination of salinomycin–Na in $CHCl_3$ solution[38] based on 500- and 600-MHz homonuclear and heteronuclear 2D NMR spectra. A simulation protocol is designed to study an operating mechanism for opening and closing of the ionophore.

Results

Improved Resonance Assignments. Resonance assignments of salinomycin–Na in $CDCl_3$ have been carried out before.[5,6] To check and revise the previous assignments, a combination of several NMR techniques (TOCSY,[39,40] NOESY,[20,30,41] E. COSY,[42,43] and HSQC-TOCSY[44–46]) was used.

The resonance assignments of the olefinic protons H18 and H19 were found to be interchanged with respect to previous reports by quantitative analysis (see further down) of the NOESY spectrum (Table I). Individual NOE-derived distances to H34, H15$^{pro\text{-}R}$, H20, and H13 unambiguously identified H18 and H19.

The second error in the previous assignment concerns the H26$^{pro\text{-}S}$ and H22$^{pro\text{-}S}$ protons. The evaluation of the HSQC-TOCSY spectrum unambiguously confirms our new assignment (Figure 2) with H22$^{pro\text{-}S}$ and H26$^{pro\text{-}S}$ correlating to C22 and C26, respectively, while the carbon assignment is established by the cross peaks to the other protons at the same carbon resonances (lines in Figure 2).

The quality of the HSQC-TOCSY correlation with respect to F_1 artifacts was improved by a homospoil pulse and two trimpulses. The new proton assignments were consistent in all spectra.

Further individual resonance assignments for each of the methyl groups (34, 37, and 39, which overlapped before[5,6]) were possible.

Extraction of Conformationally Relevant NMR Parameters. The determination of structure from NMR spectroscopy is based on distances between protons derived from proton–proton dipolar interactions. A NOESY experiment at 600 MHz with a mixing time of 600 ms provided quantitative information on interproton distances. Due to its low molecular weight, salinomycin–Na is in the positive NOE regime,[30] with all NOE cross peaks being negative toward the diagonal. The distances were calculated using the isolated two-spin approximation[47] and served as input values for the MD calculations (Table I). However, at the end of the structure determination, the results were checked for the reliability of the NOE data by a back-calculation[47–49] of the NOESY spectrum. The calculated distances (last column in Table I) show no large deviations from the experimental data.

Independently, the validity of the linear approximation for the evaluation of the NOESY spectrum with a 600-ms mixing time was checked by buildup curves taken from a series of seven NOESY spectra with mixing times varying from 100 to 1200 ms (data not shown). The analysis of the data was performed for a representative subset of the dipole–dipole pairs and reveals satisfactory results that justify the evaluation of a single NOESY with a 600-ms mixing time.

Structurally relevant coupling constants were extracted from a 1D ^1H NMR spectrum and an E. COSY[42,43] spectrum. With respect to previous reports, five additional J coupling values were determined. For rings A and D it was not possible to derive all coupling constants due to signal overlap.

Three additional diastereotopic assignments for CH_2 groups were achieved with respect to previous reports.[6,7] Hence, individual NOEs for proton H15$^{pro\text{-}R}$ served as input values for the MD calculation. The assignment of H15$^{pro\text{-}R}$ is unambiguous from $^3J_{HH}$ values and from NOESY cross peaks to H13, H18, and H19. However, NOE constraints of the residual CH_2 group protons were included in the MD calculations with correction terms because reliable prochiral assignments were obtained only in a later assignment step during the calculation.

Structure Refinement by MD Calculation. In Vacuo Simulation. In order to translate the NOE-derived distances into a three-dimensional molecular structure, restrained molecular dynamics (MD) calculations were utilized. Mutually different starting structures *START A* and *START B* were built, both with rings A and E in inverted chair conformations compared to the expected target structure. *START A* represents an almost completely elongated structure, and *START B* was built according to the X-ray structure of the *p*-iodophenylacyl ester derivative of salinomycin.[37] However, for both structures the C1/O11 distances were maximized to 13 Å. The *in vacuo* simulations were performed with salinomycin as a neutral carboxylic acid without an ion present. In the initial phase (200 ps) of both calculations, which included only a few long-range NOEs, the overall macrocylic structure is formed. During the simulations, the NOE data set could be increased (NOE sets given in Table I). Although the dynamic behavior is different, both simulations lead to nearly identical low-energy conformations which satisfy the NOE distances (Table I). The conformation with the smaller distance restraint violation (denoted *VACUUM*, Figure 3) served as starting structure for the following solvent simulation.

Restrained MD Simulation in Solution. The resulting structure *SOLV-1* (Figure 4) of the NOE-restrained MD calculation, which takes the ion and the solvent into account, is very similar to *VACUUM*. The predicted hydrogen bond O11H → O1C is formed in all minimized low-energy conformations with a donor–acceptor distance around 170 pm. A second hydrogen bond of

(34) Shoji, J.; Kozuki, S.; Matsutami, S.; Kubota, T.; Nishimura, H.; Mayama, M.; Motokawa, K.; Tanaka, Y.; Shimakoa, N.; Otsuka, H. *J. Antibiot.* **1968**, *21*, 402–409.
(35) Gachon, P.; Kergomard, A.; Veschambre, H. *J. Chem. Soc., Chem. Commun.* **1970**, 1421–1422.
(36) Berger, J.; Rachlin, A. I.; Scott, W. E.; Sternbach, L. H.; Goldberg, M. W. *J. Am. Chem. Soc.* **1951**, *73*, 5295–5298.
(37) Ebata, E.; Kasakawa, H.; Sekine, K.; Inoune, Y. *J. Antibiot.* **1975**, *28*, 118–121.
(38) Mronga, S.; Müller, G.; Fischer, J.; Riddell, F. G. Poster presentation at the 11th EENC, Lisbon, Portugal, 1992.
(39) Braunschweiler, L.; Ernst, R. R. *J. Magn. Reson.* **1983**, *53*, 521–528.
(40) Bax, A.; Byrd, R. A.; Aszalos, A. *J. Am. Chem. Soc.* **1984**, *106*, 7632–7633.
(41) Jeener, J.; Meier, B. H.; Bachmann, P.; Ernst, R. R. *J. Chem. Phys.* **1979**, *71*, 4546–4553.
(42) Griesinger, C.; Sørensen, O. W.; Ernst, R. R. *J. Magn. Reson.* **1987**, *75*, 474–492.
(43) Griesinger, C. Ph.D. Thesis, Goethe Universität, Frankfurt, FRG, 1986, App. B9.
(44) Bax, A.; Ikura, M.; Kay, L. E.; Torchia, D. A.; Tschudin, R. *J. Magn. Reson.* **1990**, *86*, 304–318.
(45) Bodenhausen, G.; Ruben, D. J. *Chem. Phys. Lett.* **1980**, *69*, 185–189.
(46) Kessler, H.; Mronga, S.; Müller, G.; Moroder, L.; Huber, R. *Biopolymers* **1991**, *31*, 1189–1204.
(47) Borgias, B. A.; Gochin, M.; Kehrwood, D. J.; James, T. L. *Prog. Nucl. Magn. Reson. Spectrosc.* **1990**, *22*, 83–100.
(48) Kessler, H.; Seip, S.; Saulitis, J. *J. Biomol. NMR* **1991**, 1, 83–92.
(49) Seip, S. Ph.D. Thesis, Technische Universität, München, FRG, 1992.

Table I. Comparison of NMR-Derived (r^{upper}, r^{lower}) and Calculated (*VACUUM*, *SOLV-1*, *SOLV-2*) Interproton Distances of Salinomycin–Na[a]

atom i	atom j	r^{upper} [b,c]	r^{lower} [b]	*VACUUM*[d]	*SOLV-1*	*SOLV-2*	r^{back_calc} [e]	NOE set
H2	$CH_2$4	388	268	335	334	341	256	3
H2	$CH_3$42	324	266	287	264	301	267	2
H3	H2	315	285	299	299	299	357	2
H3	$CH_3$40	430	360	461	432	468		2
H3	$CH_3$41	380	250	257	287	266	259	3
H6	$CH_3$39	277	223	295	273	291	252	2
H7	H2	236	214	252	257	246	247	2
H7	$CH_2$5	325	265	310	300	315	263	3
H7	H6	263	237	247	249	247	260	2
H7	$CH_3$39	324	266	310	303	298	289	2
H7	$CH_3$40	450	380	387	385	387		3
H9	H7	294	266	289	325	296	339	2
H9	H8	263	238	251	238	257	283	3
H9	H10	336	304	306	299	299	348	3
H9	$CH_3$38	324	266	295	292	284	277	2
H9	$CH_3$39	430	360	384	383	385		3
H10	H8	420	380	315	314	258	339	3
H10	H12	273	247	252	272	277	280	3
H10	$CH_3$39	292	238	300	264	292	227	1
H12	H14	336	304	303	310	306		3
H12	$CH_3$35	282	228	284	271	287	245	1
H12	$CH_2$36	335	275	199	252	242	251	3
H12	$CH_3$37	314	256	368	274	294	287	2
H12	$CH_3$38	335	275	390	376	405		2
H13	H10	261	235	266	229	266	275	1
H13	H12	263	237	258	255	252	264	2
H13	H14	367	333	300	297	301		3
H13	H15^{proR}	294	266	245	243	257	257	2
H13	$CH_3$35	324	266	300	291	295	296	2
H18	H13	225	205	254	232	258	286	2
H18	H15^{proR}	278	252	249	244	243	285	2
H18	H20	330	300	393	398	398		2
H18	$CH_3$34	354	294	342	336	348	248	2
H19	$CH_3$34	438	368	502	461	499	286	2
H19	$CH_3$42	560	480	499	508	648		1
H19	H15^{proR}	441	399	489	481	482		2
H19	H2	420	340	333	319	426		1
H19	H20	273	247	270	265	268	313	2
H20	H7	294	266	554	430	509		1
H20	$CH_2$22	335	275	261	248	240	300	2
H20	$CH_2$26	380	320	465	417	464		1
H20	$CH_3$34	420	350	463	428	468		3
H20	$CH_3$42	500	430	503	438	633		3
H25	$CH_2$23	335	275	284	290	289	260	3
H25	$CH_2$27	324	266	319	297	326	340	3
H25	$CH_3$30	282	228	303	277	294	252	3
H25	$CH_3$33	303	247	303	304	313	292	2
H29	H25	367	337	382	363	375	396	2
H29	$CH_3$32	305	247	305	293	306	273	3
H29	$CH_3$33	500	428	485	452	473		3
$CH_3$30	$CH_3$33	427	337	484	428	485		2

[a] The constraints are assigned to the three different refinement stages (NOE sets 1, 2, and 3) according to the outlined simulation protocol. All distances are given in picometers. [b] For determination of r^{upper} and r^{lower} from experimental data, see text. [c] For CH_2 protons (except $CH_2$15), r^{upper} was increased by 100 pm. [d] For the *in vacuo* simulation the head group of the molecule was changed to the protonated carboxylic acid excluding the ion. [e] For extraction of distance information the back-calculated spectrum was calibrated in the same way as the experimental spectrum. Distances not given here were not observed as cross peaks in the back-calculated spectrum.

O8H → O2C (around 185 pm) strengthens the head-to-tail connection. Therefore, both oxygens of the carboxylic head group contribute to the closure of the complex structure as hydrogen bond acceptors.

The ion complexation pattern is best defined as a distorted pentagonal pyramid with O2, O4, O5, and O10 forming a common plane, O11 being slightly exposed under the plane, and ligand O9 representing the top of the pyramid (Figure 5). All oxygen–ion distances are around 230 pm.

For the previously assigned hinge torsions, which are assumed to be the torsions around C11 and the angle C23–C24–C25–C26,[5,6] severe restriction of conformational freedom is observed because no remarkable dihedral angle fluctuations appear during the restrained MD trajectory (Figure 6) for *SOLV-1*.

Free Dynamics. Structure *SOLV-1* was subjected to a 200-ps MD calculation in the absence of NOE constraints. The structure underwent no significant changes and is now referred to as *SOLV-2*. Hence, *SOLV-1* is established to be a low-energy conformation, with moderately increased molecular flexibility during the free MD run. Only the dihedral angles of the supposed hinge torsions adjacent to C11 show slightly increased fluctuation.

Free Dynamics without Sodium Ion. Removing the sodium ion from *SOLV-2* mimics the release at the biomembrane. During the initial phase of the 200-ps simulation in $CHCl_3$, the macrocycle opens immediately. This is shown by the head-to-tail distances C1–O11 over the trajectory (Figure 6). The torsion angles deviate from their equilibrium values in chronological order. The changes at C6–C7–C8–C9 shift ring A with its carboxylic group out of the macrocycle. The head of the molecule is then affected at O1–C1–C2–C3. Finally, the major change at C10–C11–C12–C13 occurs. This torsion angle changes from +60° to −60° via 180°, which is the major change in the unfolding process. All other open-chain torsions remain at their analyzed values.

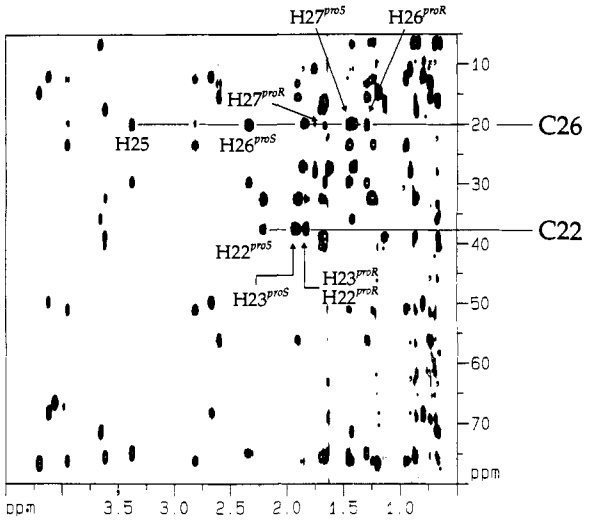

Figure 2. Part of the HSQC-TOCSY spectrum of salinomycin–Na in $CDCl_3$ at 600 MHz. Many proton resonances along F_2 at the given carbon frequency confirm that the $H26^{pro\text{-}S}/H22^{pro\text{-}S}$ assignment is interchanged with respect to previous reports.[5,6]

Discussion

The experimental data are in good agreement with the results from MD simulation for *VACUUM*, *SOLV-1*, and *SOLV-2* (Table I). Therefore, the assumptions for the interpretation of the observed NOE effects for this small, rapidly tumbling molecule are reasonable. Precise statistical data analyses of the calculated structures are given in Tables II and III.

A contribution to the average restrained violation (ARV) given in Table III is achieved when the difference between the actual distance in *VACUUM*, *SOLV-1*, or *SOLV-2* and the r^{upper} and r^{lower} boundary of an individual NOE exceeds the range defined by r^{upper} and r^{lower}. It is obvious that the restrained MD simulation, with explicit treatment of the solvent surrounding and consideration of the sodium ion, resulted in the most reasonable conformation (*SOLV-1*) with the lowest distance restraint violation (Table III). While the vacuum-derived structure *VACUUM* demonstrates an averaged restraint violation of 21.4 pm, this target value is decreased for *SOLV-1* to 12.4 pm. It is not surprising that this value is increased for *SOLV-2*, as this structure was obtained by a MD simulation with experimentally derived restraints not taken into account.

The H20/H7 NOE is the most violated constraint. As with some other NOEs for large distances (Table I), this NOE is not observed in the back-calculated spectrum. The H20/H7 NOE in the experimental NOESY spectrum might be a composition of the direct H20/H7 NOE and a relayed NOESY correlation via a H7/HO8 NOE with a succeeding HO8/H20 exchange step. The possible relayed NOE contribution might increase the NOE intensity and falsify the H20/H7 distance to the small value (Table I) that cannot be fullfilled by the overall salinomycin structure. The argument for the hypothetical relay step relies on the additionally observed HO8/H20 exchange peak.

A superposition of the calculated structures obtained during the MD run of *SOLV-1* provides no further insight as the structure fluctuates only moderately around the derived minimum conformation. For the most flexible torsions this can be seen from row 1 in Figure 6. We choose the comparison of the rms deviations for pairwise superposition of the different discussed conformations *VACUUM*, *SOLV-1*, and *SOLV-2* and the starting conformations (Table II) to be more informative. The comparison reveals the close structural relationship between the refined structures, which are completely different from the starting structures. Both starting structures are mutually different, too.

A detailed description of the conformational behavior of salinomycin–Na in solution was possible with a higher degree of confidence with respect to earlier structural analyses of carboxylic ionophore cation complexes[1,5,6] (Figures 4, 5).

In *VACUUM* (Figure 3), ring A and ring E adopt the expected chair conformation, simplifying the formation of the head-to-tail hydrogen bond. Previously the O8H donor was assigned to the O4H acceptor group only. However, we now find a dynamic behavior of the donor O8H alternating between the acceptor sites O2 and O4. Concerning the Na coordination (Figure 5), we are confident in excluding O6 and O8 from the first coordination shell of the cation, which is in contrast to previous reports.[5,6] The contribution of the carboxylic O2 atom to the metal coordination shell is presur ibly forced by the unexpected O8H → O2 hydrogen bond. This ecise analysis of the hydrogen bond pattern is possible only frc the solvent simulation.

The dihedral analysis of *VACU* /M and *SOLV-1* is consistent with the conformation proposed l Anteunis and Rodios in 1981 based on CH–CH fragment conf mations from $^3J_{HH}$ values.[5,7] Their data set was confirmed and tended. The data allow each torsion to deviate by less than 3 ° from its idealized value.

The different orientation of al of the ethyl substituents with respect to the proposed conform tion of Anteunis and Rodios stems from the fact that our calcu tions were performed without diastereotopic assignments of H , H36, and H41 protons and without dihedral restraints base on coupling constants.

As a result of a comparative con rmational study of 15 different polyether antibiotics, Anteunis *et al.* defined the torsions around C11 together with C23–C24–C25–C26 to be the major hinges for the function of the ionophore.[7] However, using a $^3J_{HH}$ interproton path, the torsions C9–C10–C11–C12 and C10–C11–C12–C13 are not directly accessible. Hence, our detected deviations in *SOLV-1* (similar in *VACUUM*) from the idealized values are understandable. The MD trajectories of the restrained and free MD calculation in solution (Figure 6) allow us to define the C10–C11–C12–C13 and the C6–C7–C8–C9 angles to be the major hinge torsions. This unambiguously excludes two of the previously proposed hinge angles due to their restrictions in flexibility.

Conclusion

The first ionophore metal complex structure determined by NMR in solution based on NOE-derived distances and refined by MD calculation is reported. The conformational space of salinomycin is restricted by complexing the sodium ion with a coordination pattern of a distorted pentagonal pyramid including one of the carboxylic O atoms. The ion acts as a structural template which induces a macrocyclic conformation of the ligand. The macrocyclic structure is completed by a head-to-tail O11H → O1C hydrogen bond. Although the coordination patterns of a lot of ionphores are known from crystal structural analyses,[1] even for valinomycin or monensin a solution structure using NOE distance constraints has not yet been determined. Here, we provide novel direct evidence for the coordination pattern in solution by the description of the NOE-derived solution structure.

For salinomycin, a dynamic model allows both the definition of the major hinge torsions that are responsible for the operating mechanism and a chronology of the unfolding path.

Evaluation of the molecular surface lipophilicity defines an overall hydrophobic skin and a hydrophilic core burying the ion. We identify the O8H → O2 and O8H → O4 three-center hydrogen bond as the hydrophilic interface in the overall hydrophobic surface of the complex for the interaction with polar components at the membrane surface, where the ion is released.

Experimental Section

(a) NMR Measurements. Salinomycin–Na (10 mg) was dissolved in 0.5 mL of degassed $CDCl_3$. All NMR spectra were recorded on Bruker AMX600 or AMX500 spectrometers at 300 K, with the exception of the

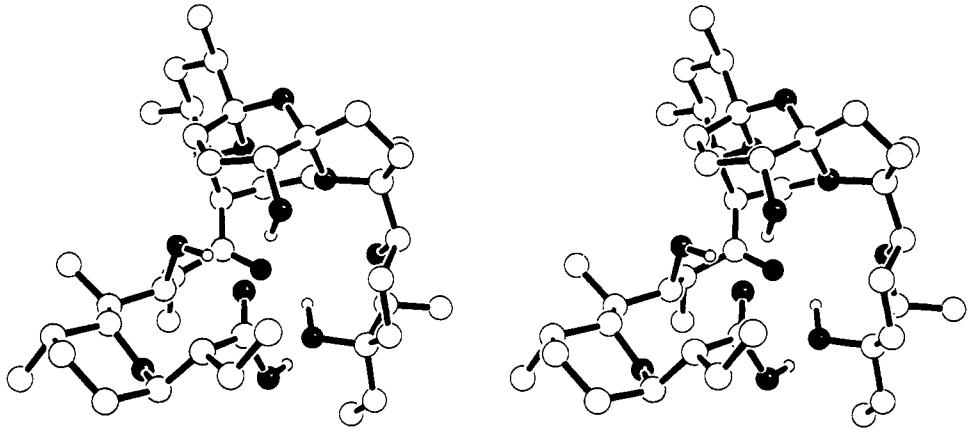

Figure 3. *In vacuo* derived conformation *VACUUM* of salinomycin.

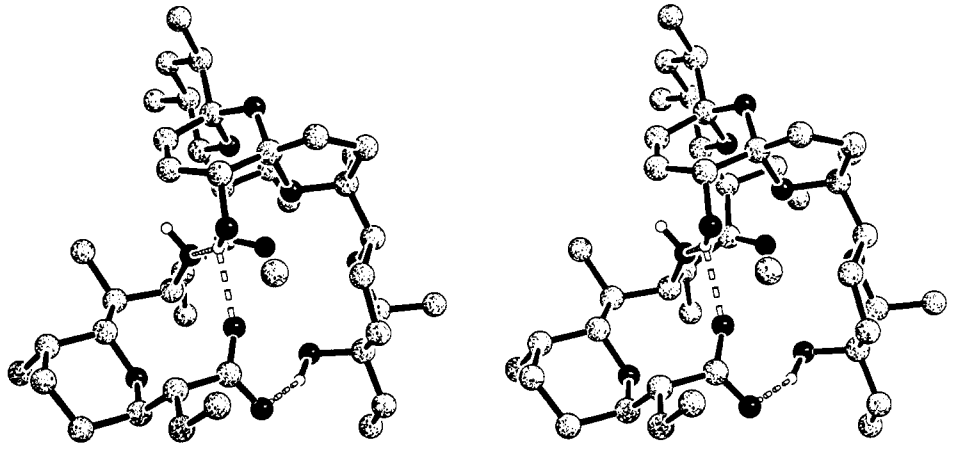

Figure 4. Solution structure of salinomycin–Na, obtained as the equilibrium conformation *SOLV-1* after restrained MD calculation in solution. The double head-to-tail H-bonding is indicated.

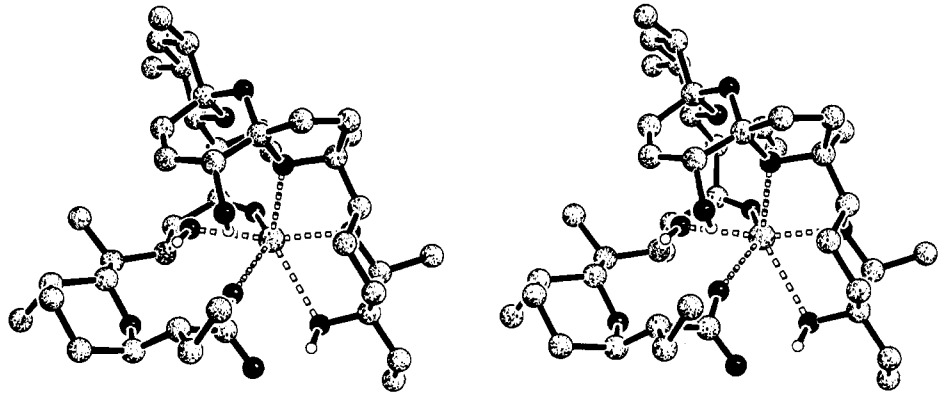

Figure 5. Metal ion coordination pattern of salinomycin–Na, representing a distorted pentagonal pyramid.

NOE buildup curve recorded at 305 K. All 2D spectra were recorded and processed in the phase-sensitive mode with quadrature detection in both dimensions. Parameters not mentioned here were set as usual.[50]

(1) 1D ^{1}H NMR spectrum (600 MHz): size 8*K*; sweep width 4464 Hz; 8 scans.

(2) TOCSY spectra (500 MHz): pulse sequence $D1$–90°–t_1–MLEV17–t_2; relaxation delay $D1$ = 6 s; 8 scans per each of 512 t_1 increments; size in acquisition domain 2*K*; duration of spin-lock period 80 ms.

(3) E. COSY spectrum (600 MHz): pulse sequence $D1$–90°–t_1–90°–$D2$–90°–t_2; phase cycling according to ref 43; $D1$ = 6s, $D2$ = 2 μs; sweep width in F_1 and F_2 5000 Hz; 36 scans per t_1 increment. For the extraction of *J* couplings, strip processing was applied to the interesting regions with zero-filling up to 8*K* and 4*K* in t_2 and t_1, respectively, before Fourier transformation.

(4) NOESY spectra: pulse sequence $D1$–90°–t_1–90°–τ_{mix}–90°–t_2; relaxation delay 6 s; 90° pulse, 11.2 μs with attenuation of 3 dB; 16 scans per each of 512 t_1 increments; sweep width 7.5 ppm; at 600 MHz, mixing time 600 ms; at 500 MHz, a series of seven NOESY spectra with different mixing times of 100, 200, 400, 600, 800, 1000, and 1200 ms were recorded. Calibration of the NOESY spectrum to extract distance constraints was done by setting the H6/H40 NOE cross peak to 240 pm.[51]

(5) HSQC-TOCSY spectrum (600 MHz): pulse sequence $D1$–90°–(^{1}H)–$D3$–180°(^{1}H,^{13}C)–$D3$–$P5$–90°(^{1}H)–$P10$–$D5$–90°(^{13}C)–t_1/2–180°(^{1}H)–t_1/2–90°(^{1}H,^{13}C)–$D3$–180°(^{1}H,^{13}C)–$D3$–$P5$–MLEV–17–t_2; sweep width in F_1(^{13}C) = 22 727 Hz (150 ppm) and in F_2(^{1}H) = 4464 Hz; 90°(^{1}H) pulse, 30 μs with attenuation of 9 dB; 90°(^{13}C) pulse,

(50) Kessler, H.; Mronga, S.; Will, M.; Schmidt, U. *Helv. Chim. Acta* **1990**, *73*, 25–47.

(51) Kessler, H.; Kerssebaum, R.; Klein, A. G.; Obermeier, R.; Will, M. *Liebigs Ann. Chem.* **1989**, 269–294.

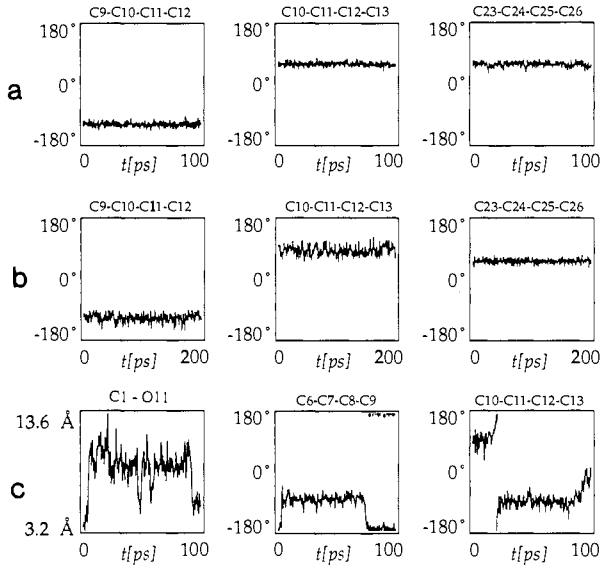

Figure 6. Open-chain dihedral angles followed during the first 100 ps of the restrained dynamics *SOLV-1* (a) and *SOLV-2* (b) and the free dynamic in solution (c) without ion. Only slightly more flexibility is observed in *SOLV-2*, but during the free dynamics a chronological order of the macrocycle ring-opening mechanism is observed, including the rapidly elongating C1–O11 distance.

Table II. Root Mean Square Deviations of the Two Different Starting Structures (*START A*, *START B*), the Vacuum-Derived Conformation (*VACUUM*), and the Structures Refined in a Solvent Box (*SOLV-1*, *SOLV-2*)[a]

	START A	*START B*	*VACUUM*	*SOLV-1*	*SOLV-2*
START A		357	374	386	377
START B	406		219	225	218
VACUUM	425	301		55	38
SOLV-1	435	300	76		48
SOLV-2	429	297	60	56	

[a] Values are given in picometers for pairwise superposition of only the main-chain atoms (above the diagonal) and of all heavy atoms (below the diagonal). The main chain atoms are defined along the master torsion definition path (compare to legend of Figure 1) through the molecule.

Table III. Distance Restraint Violation Analysis for the Discussed Conformations *VACUUM*, *SOLV-1*, and *SOLV-2*[a]

conformation	N_{viol}[b]	ARV[b]	N_{viol} (>20 pm)[c]	⟨viol⟩ ± σ_{viol}[c]	Δ_{min}[c]	Δ_{max}[c]
VACUUM	27	21.4	15	50 ± 20	21	85
SOLV-1	24	12.4	13	35 ± 15	21	68
SOLV-2	31	24.5	15	63 ± 31	32	133

[a] The number of violated restraints is given by N_{viol} and the averaged restraint violation by AVR. When a tolerance of 20 pm is applied, the number of violated restraints is reduced to N_{viol}(>20 pm). Average and standard deviation ⟨viol⟩ ± σ_{viol} is calculated over all violated distance restraints that deviate by more than 20 pm from the defined distance range. Δ_{min} and Δ_{max} refer to the minimum and maximum restraint violations. All distance values are given in picometers. [b] N_{viol} and ARV are calculated by averaging over all 51 applied distance restraints without any cutoff. [c] For the statistics, the NOE between H20 and H7 is not taken into account.

11.1 μs; trim pulse *P*5 = 3 ms; homospoil pulse *P*10 = 2 ms; relaxation delay *D*1 = 6 s; recovery delay *D*5 = 2 ms; 80-ms TOCSY spin-lock period; sizes in F_1 and F_2 were 256 and 2*K* data points, respectively; INEPT delay for evolution and refocusing of $^1J_{CH}$ $D3 = {}^1/_4J_{CH} = 1.7$ ms. Two trim pulses (*P*5) and the homospoil pulse (*P*10) with succeeding recovery delay *D*5 reduce artifacts along F_1 in comparison to the sequence without those pulses.

(b) Back-Calculation of the NOESY Spectrum. The calculation was performed with the homewritten program of S. Seip,[49] which is based on ref 47 and on eq 1–6 in ref 48. As input data served: (a) the DISCOVER coordinate file of the final structure, (b) chemical shift values of all nonlabile protons, (c) correlation time of 100 ps (due to resonance overlap, τ_c could not be determined by the method using integrated cross and diagonal peaks,[52,53] τ_c was estimated to be 100 ps, (d) leakage was estimated to be 0.1 s, (e) sweep width and transmitter frequency were set as in the experimental data set.

(c) Computational Procedure of MD Calculations. All molecular mechanics simulations were carried out on Silicon Graphics 4D/25TG, 4D/70GTB, and 4D/240SX computers using the Consistent Valence Force Field (CVFF)[54,55] implemented in the DISCOVER (Biosym) software package Version 2.70 together with the INSIGHT II Version 2.0.2a as graphic interface. For all energy minimizations (EM) and molecular dynamics (MD) simulations, no cross terms describing the coupling of different internal coordinates were used.[54,55] Upper and lower limit constraints r^{upper} and r^{lower}, respectively, were obtained from integrated and calibrated 2D NOESY cross peak intensities by averaging the values from above and below the diagonal and allowing a tolerance ±5% (Table I). As a penalty term for the violation of the NMR-derived distance constraints, a skewed biharmonic function was applied. The harmonic potential switches at the maximum force of 100 kcal mol^{-1} Å^{-1} to the modified harmonic form. We performed restrained EM and MD calculations with a force constant *k* of 3978 kcal mol^{-1} Å^{-2} at 500 K and 2387 kcal mol^{-1} Å^{-2} at 300 K. For all simulations a time step for integrating Newton's equation of motion of 1 fs was used together with the Verlet algorithm.[56] The neighbor list was updated every 10 steps. The trajectories were updated every 250 steps to obtain 400 structures for a 100-ps simulation period. For all solvent MD calculations the cutoff radius for nonbonded interaction was 13 Å, with a switching distance of 2 Å. For the *in vacuo* simulations the head group of the molecule was changed to the protonated carboxylic acid, excluding the sodium ion. For generation of the coordinates of the two starting structures, the program INSIGHT (Biosym) was used. The manually built conformations were minimized (steepest descent algorithm)[57] for 1000 steps. Next, a 200-ps restrained MD simulation was performed at 500 K with a selected number of NOE constraints (NOE set 1 in Table I). For the next 100 ps at 300 K, further NOEs were included (NOE set 2 in Table I). From the resulting target structure, additional NOE connectivities could be assigned, increasing the number of distance constraints from 34 to 51 (NOE set 3 in Table I) for the next 100-ps MD simulation at 300 K. The same concept was used for both starting structures. Five low-energy conformations were taken every 20 ps from the last 100-ps trajectory and minimized (conjugate gradient algorithm),[58–60] leading to a conformational family.

After modification of the head of the ionophore to the carboxylate anion and inclusion of the sodium ion into the hydrophilic cavity, the system was soaked in a solvent box of 139 $CHCl_3$ molecules with a box length of 30 Å. A full effective charge was left for the ion with the Lennard-Jones parameters C12 = 14 000 kcal Å^{12} mol^{-1} and C6 = 300 kcal Å^6 mol^{-1}. Next, 1000-step EM (steepest descent algorithm)[57] and further 100-step EM (conjugate gradient algorithm)[58–60] were performed. In the following 100 ps of restrained MD simulation at 300 K, periodic boundary conditions were applied. The resulting structure *SOLV-1* served as the starting structure for recording a 200-ps free dynamic simulation to study the dynamics of the complex and to test if *SOLV-1* is a low-energy conformation. For the investigation of the unfolding mechanism, the sodium ion was removed and additional unrestrained 200-ps free MD simulations were performed.

Acknowledgment. We thank Prof. Dr. H. Kessler for special support and Prof. Dr. C. Griesinger for help with the evaluation of the E. COSY spectrum and with the interpretation of the NOE buildup data. We thank Dr. S. Seip for the permission to use his self-written back-calculation program.[49] Dr. U. Anders

(52) Reggelin, M.; Hoffmann, H.; Köck, M.; Mierke, D. F. *J. Am. Chem. Soc.* **1992**, *114*, 3272–3277.
(53) Esposito, G., Pastore, A. *J. Magn. Reson.* **1988**, *76*, 331–336.
(54) Maple, J. R.; Dinur, U.; Hagler, A. T. *Proc. Natl. Acad. Sci. U.S.A.* **1988**, *85*, 5350–5354.
(55) Dauber-Osguthorpe, P.; Roberts, V. A.; Osguthorpe, D. J.; Wolff, J.; Genest, M.; Hagler, A. T. *Proteins: Struct. Funct. Genet.* **1988**, *4*, 31–47.
(56) Verlet, L. *Phys. Rev.* **1967**, *159*, 98–103.
(57) Wiberg, K. B. *J. Am. Chem. Soc.* **1965**, *87*, 1070–1078.
(58) Williams, J. E.; Stang, P. J.; Schleyer, P. v. R. *Annu. Rev. Phys. Chem.* **1968**, *19*, 531–558.
(59) Fletcher, R. *Practical Methods of Optimization*; John Wiley & Sons: New York, 1980; Vol. 1.
(60) van Gunsteren, W. F.; Kaplus, M. *Macromolecules* **1982**, *15*, 1528–1544.

is gratefully acknowledged for recording the NOESY spectra for the NOE buildups. G.M. thanks the Fond der Chemischen Industrie for a fellowship. We are indebted to Dr. D. Dost (Hoeschst AG, Frankfurt) for providing a sample of salinomycin–Na. PD Dr. W. Braun (ETH, Zürich) is acknowledged for carefully reading the manuscript.

Supplementary Material Available: Tables of proton chemical shifts and coupling constants, oxygen atom–Na ion distances in *SOLV-1* and *SOLV-2* for Na coordination pattern analysis, and a list of the master torsion values in the compared structures (4 pages). Ordering information is given on any current masthead page.